# Estimating Near Electric Field of Polyhedral Gold Nanoparticles for Plasmon-Enhanced Spectroscopies

José Luis Montaño-Priede[†] and Umapada Pal[*,‡]

[†]Department of Physics & Astronomy, University of Texas at San Antonio, One UTSA Circle, San Antonio, Texas 78249, United States

[‡]Instituto de Física, Benemérita Universidad Autónoma de Puebla, Apdo. Postal J-48, Puebla, Pue. 72570, Mexico

**S** *Supporting Information*

**ABSTRACT:** Technological application of polyhedral plasmonic nanoparticles (NP) is closely associated with their strong ability of localizing electric field at and near the surface. In this study, we calculate the optical properties of most common regular polyhedral Au nanoparticles such as the cube, rhombic dodecahedron, pentagonal bipyramid, and octahedron and compare with the optical properties of spherical particles to investigate the plasmonic behavior of metallic nanoparticles due to the breakdown of spherical symmetry. We demonstrate that the highest electric field enhancement (1 order magnitude higher than the spherical NP) occurs in octahedral Au NPs as the consequence of strong localization of incident electromagnetic field, decreasing the diffraction limit of the optical microscopies, which depends both on their size and orientation with respect to the polarization of incident light, increasing the system resolution. Higher order modes (quadrupole, hexapole, octupole, etc.) appear along the dipole mode as the shape of the NPs deviates from their regular spherical shape, even though their size remains much smaller than the incident wavelength. Irrespective of their shape, the major contribution of small NPs comes from the light absorption. Although the scattering efficiency of Au NPs becomes significant with the increase of their size, the NPs with sharper borders and vertices scatter higher fraction of light than the NPs of spherical shape.
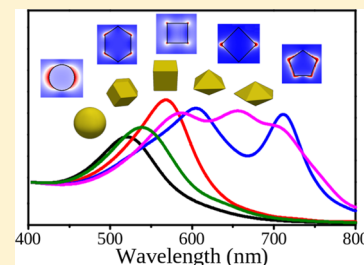
## INTRODUCTION

Electric field enhancement at the nanoscale has become a subject of intense current research for the technological applications of plasmonic nanostructures, especially for improving the sensitivity and response in single molecular detection, renewable energy transducers, hyperthermia therapy, etc.[1−3] A strong electric field is generated around metallic nanoparticles when the conduction electrons of the metal coherently oscillate (plasmon) in resonance with an incoming electromagnetic (EM) radiation of specific wavelength, known as localized surface plasmon resonance (LSPR).[4] The intensity of the electric field and the resonance wavelength, where the maximum of the electric field is expected, are mainly determined by the composition, structure, and shape of the nanoparticles, along with the nature of medium surrounding them.[5,6] In principle, one can tune the LSPR, both its position and intensity, by controlling the aforementioned parameters of metal nanoparticles. In fact, researchers could fabricate shape-tuned polyhedral plasmonic nanoparticles to tune the LSPR,[7−9] demonstrating their improved response in surface-enhanced Raman spectroscopy (SERS).[10,11] For example, Chen et al. reported a synthesis route to obtain cubic, rhombic dodecahedral, and octahedral nanoparticles through chemical reduction of gold ions in *N,N*-dimethylformamide solution in the presence of poly(vinyl pyrrolidone), using NaOH solution as the shape controlling agent.[12] On the other hand, Zhang et al. fabricated octahedral gold nanoparticles by thermal decomposition of gold salt in block co-polymers (polystyrene-

block-poly(2-vinylpyridine)) to use them as SERS substrates for molecular detection.[11] The SERS signal detected by their octahedral gold nanoparticles was seen to be 3 times higher than the signal detected by spherical Au nanoparticles. Recently, Kuo et al. have reported the fabrication of Au NPs of different morphologies such as rhombic dodecahedrons, cubes, and octahedrons by varying the concentration of Au precursor.[13] In fact, there exist a vast number of experimental and theoretical research reports in the literature on the control of LSPR of plasmonic nanostructures (Au and Ag, mainly), dealing their far-field behaviors and their implications in optical and optoelectronic devices.[14−16] On the other hand, although several research groups have fabricated plasmonic nanostructures of specific shapes[17−21] and evaluated their near-field behaviors both experimentally and theoretically,[4,22,23] demonstrating the high near-field enhancement in plasmonic nanostructures of specific shapes, a systematic study on how the near electric field depends on the shape and size of small plasmonic nanostructures, affecting their molecular sensing performance through SERS, is lacking.

Therefore, in the present work, we studied the near electric field (NEF) enhancement in the most common polyhedral gold nanoparticles of different sizes to draw the relation between the developed electric field around their surface,

which can serve as a guide for the fabrication of gold nanoparticles with optimum SERS response.

## ■ THEORETICAL CONSIDERATIONS

A finite differences time domain (FDTD)-based simulation software (MEEP)[24] was used in this work to calculate the optical properties of Au NPs in the far- and near-field regions. Five different morphologies (polyhedral) of Au NPs, each of four sizes, were considered, as shown in Table S1. The morphologies considered were sphere (Sph), cube (Cub), octahedron (Oct), pentagonal bipyramide (PBp), and rhombic dodecahedron (RhD); which are the most-frequent experimentally reported shapes of Au nanostructures.[12,17−21,25]

To compare the optical properties of the Au NPs of different morphologies, the size of the particles was established in relation to the equivalent volume of the sphere, expressed by equivalent sphere radius ($R_{eq}$, Table S1), covering the size range from 10 to 50 nm, which is the most usual size range of Au NPs fabricated experimentally. For example, a Sph Au NP of $R_{eq}$ = 5 nm has a volume of 523.6 nm$^3$. So, the other polyhedrons of equal volume will be considered equivalent to this spherical NP. For simulation, the refractive index of gold was taken from ref 26, and water was taken as the surrounding medium ($n_m$ = 1.333).

The size of the FDTD computational cell was determined as 4 times the size of the analyzed nano-object, using a perfectly matched layer of 50 nm thickness as the boundary condition of the cell. The values of the two most important parameters used to simulate the electrodynamic systems with FDTD, the spatial resolution ($\Delta_x$), and the Courant number ($c = \Delta_t/\Delta_x$) are specified for each nano-object in Table S1. As the spatial resolution was reduced intentionally for the bigger NPs to reduce the computation time (the established time to compute the optical response for each NP was from 1 to 2 weeks, without compromising the reliability of the results), the Courant number was also varied depending on the resolution ($\Delta_t < c\Delta_x$).

The incident EM wave (Gaussian source) was chosen to propagate in the $z$-direction with the polarized electric field in the $x$-direction with the wavelength range from 400 to 800 nm and unitary amplitude. Table S1 shows schematically the shapes of the Au NPs considered (first column, left side) and the position of the polyhedral NPs with respect to the incident EM wave (first column, right side). Electromagnetic monitors were used to calculate the scattering ($C_{sca}$) and the absorption ($C_{abs}$) cross-sections and the NEF. The extinction cross-section was calculated as the sum of the aforementioned cross-sections, i.e., $C_{ext} = C_{abs} + C_{sca}$. The efficiency factors were determined dividing the optical cross-sections with the physical cross-section of the specific nano-object (using the equivalent radius, e.g., $Q_{ext} = C_{ext}/\pi R_{eq}^2$). The simulations were terminated when the field intensity in the simulation was decayed by $1 \times 10^{-10}$ times of the initial amplitude. Finally, electric charge density was calculated from the Maxwell equation $\rho = \text{div}(D)$, where $\rho$ is the charge density and div($D$) is the divergence of the electric displacement field.

## ■ RESULTS AND DISCUSSION

As it has been well established (see e.g., refs 4 and 5), the extinction spectra of spherical gold nanoparticles can be tuned in the visible wavelength region by tuning their size and the surrounding medium, and this is not an exception when the

shape of the nanoparticle is changed from the simplest spherical to other. Figure S1 (Supporting Information) shows the calculated extinction efficiency factors for the considered morphologies of Au-NP: sphere, rhombic dodecahedron, cube, octahedron, and pentagonal bipyramid, for four equivalent radii (Table S1): 5, 15, 35, and 50 nm. For all of the nanoparticles, the position and the bandwidth of LSPR increased with the increase of size, regardless of their morphology, mainly because of the retardation effect of the plasmon, i.e., the energy dispersion probability of the oscillating electrons (due to collisions) increases with the nanoparticle size.[5]

Figure 1 shows the extinction efficiency factors of Au NPs of different shapes for $R_{eq}$ = 5 nm, in which the band associated to
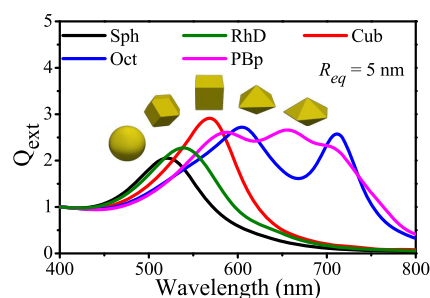


**Figure 1.** Extinction efficiency factors of gold nanoparticles of different shapes: sphere (Sph), rhombic dodecahedron (RhD), cube (Cub), octahedron (Oct), and pentagonal bipyramid (PBp) of 5 nm equivalent radius ($R_{eq}$).

the LSPR is modified depending on the morphology. The Sph, RhD, and Cub nanoparticles present only one LSPR band associated (at first sight) to the dipole mode, with a gradual red shift in peak position following the order, for all of the considered sizes (see Figure S1). A similar observation has also been reported for these particular shaped Au NPs in their corresponding absorption spectra.[27,28] On the contrary, the Oct and PBp NPs present multipolar mode bands, even though they are in the quasi-static regime (the NP size is much smaller than the applied light wavelength). As has been observed by Li et al.[29] for their synthetized Oct Au NPs of sharp edges with $R_{eq}$ less than 50 nm, we observed two LPSR bands for Oct Au NPs (Figure S1). Very similar observation has also been made for the PBp NPs; however, the multiple polar mode bands are overlapped due to their lesser sharp edges, as confirmed by Zhang et al.[30]

To determine the nature of the polar modes for all of the resonances showed in Figure 1, electric charge density ($\rho$) distribution in the $xy$ plane was calculated for the five NPs with $R_{eq}$ = 5 nm (Figure S2), where the red and blue colors represent the positive and negative charge distributions, respectively (represented by + and − symbols). The dipole mode is clearly visible in the Sph NP (Figure S2a), where the positive and negative charges form two symmetrical halves of the NP polarized along the direction of the incident electric field. The polar mode is not visibly clear in the case of RhD and Cub NPs (Figure S2b,c) as the plasmon is divided into two region pairs (at the bottom and top of the NPs separated by the region in the middle with almost zero charge). Nevertheless, both the region pairs have same polarization (same phase, − + and − +), and consequently, it is considered a dipole mode (RhD NP presents two more small region pairs
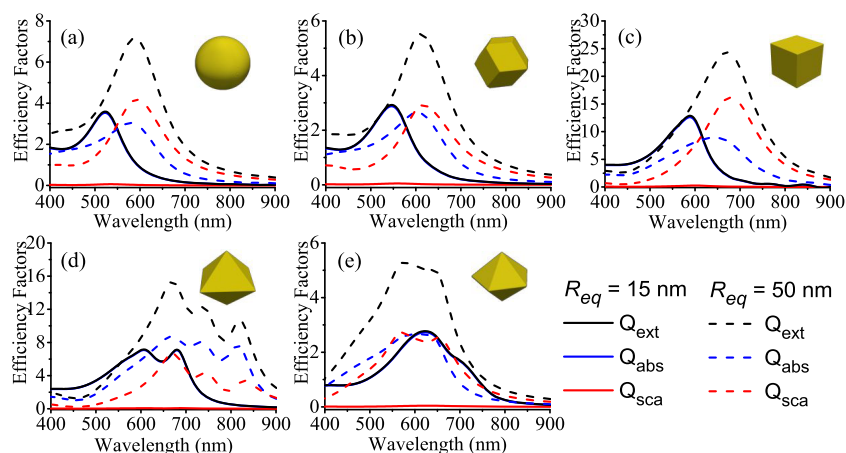
**Figure 2.** Extinction ($Q_{ext}$, black lines), absorption ($Q_{abs}$, blue lines), and scattering ($Q_{sca}$, red lines) efficiency factors of gold nanoparticles of (a) sphere, (b) rhombic dodecahedron, (c) cube, (d) octahedron, and (e) pentagonal bipyramid shapes for equivalent radius ($R_{eq}$) of 15 nm (solid lines) and 50 nm (dashed lines). Since $Q_{ext} = Q_{abs}$ for $R_{eq}$ = 15 nm ($Q_{sca} \sim 0$), so the black solid line hides the blue one.

with opposite polarization, but we consider their contribution negligible; conversely, the mode would be hexapole). In the case of the Oct NP, the dipolar nature of the largest resonant wavelength (710 nm) is also clear, where the positive and negative charges are concentrated at the vertices along the applied electric field direction (Figure S2d). The charge distribution for the second mode (605 nm) shows three dominant region pairs of charges (+ −, − +, and + −); two pairs with same polarization at the bottom and top of the image and one at the middle with different polarizations, concluding that the polar mode is hexapole. Finally, the PBp NP shows the dipole (− +), quadrupole (− + and + −), and octupole (+ −, − +, + −, and − +) modes since it has one, two, and four region pairs for each resonance with alternating polarizations (Figure S2e).

Although there exists no theory which relates the morphology of metallic NPs to the characteristics of their LSPR bands, we can see from Figures 1 and S1 that more similar is the shape of the NPs to a sphere, its LSPR band is closer to that of a spherical NP.[31] For example, the shape of an icosahedral NP (regular polyhedron consisting of 20 triangular faces, not considered in the present work) is too close to that of a spherical NP, and hence the optical properties of an icosahedral NP are very similar to that of a spherical NP.[14] Therefore, as the shape of a NP approaches to a sphere, the bands of higher order modes overlap with the dipole one, and the LSPR position is blue shifted, as shown in Figures 1 and S1.

The light extinction by metallic nanoparticles is the result of light absorption and scattering. The major contribution in the extinction efficiency of small NPs comes from the absorption (Figure 2). On the other hand, the contribution of scattering on the extinction efficiency factor increases as the size increases (Figure 2). However, the two phenomena are independent, regardless of the shape of the small (zero-dimensional) nanoparticles. Nevertheless, the relative intensities of absorption and scattering efficiency factors depend on NP morphology, when their size is relatively large. In the case of larger Sph, RhD, and Cub NPs, the light scattering is more intense than the light absorption (Figure 2a−c, respectively). Conversely, light absorption is more intense than scattering in Oct NPs (Figure 2d), and the absorption and scattering are similar in PBp NPs for the same spectral range (Figure 2e).

Now let us address the optical properties of the considered polyhedral nanoparticles in the near-field region. Figure 3
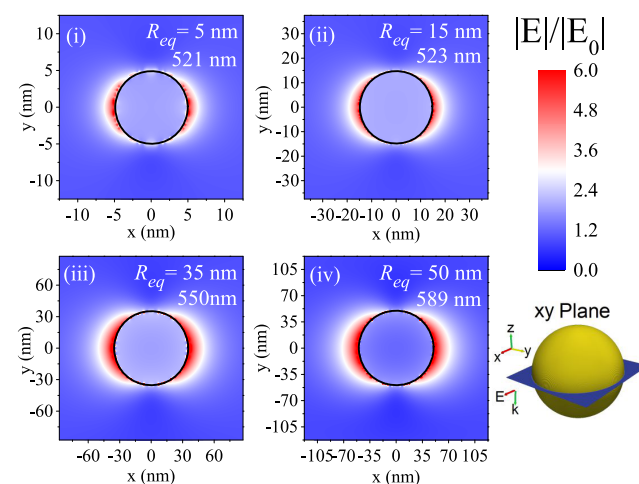


**Figure 3.** Spatial distribution maps of a near electric field for the spherical gold nanoparticles in the $xy$ plane (see inserted image) for $R_{eq}$ of (i) 5 nm, (ii) 15 nm, (iii) 35 nm, and (iv) 50 nm.

shows the spatial distribution of the near electric field intensity ($|E|/|E_0|$) in the $xy$ plane for the Sph NP excited by the maximum of LSPR wavelength ($\lambda_{LSPR}$). As can be noticed (Figure 3), the NEF corresponds to dipole mode (as we explained earlier with the $\rho$ map, Figure S2a) for all of the four sizes intensify at the NP surface, in parallel to the $x$-axis (perpendicular to the direction of excitation), with maximum intensities 3.5−6 times higher than the incident electric field. The value of $|E|/|E_0|$ increases progressively with the increase of the size of the NP (Sph). The electric field decays quickly from the surface to a few nanometers, at the rate proportional to $r^{-3}$.[32]

In the case of a RhD gold NP (Figure 4), the near electric field is concentrated at the vertexes (and partly in the edges) of the NP. Such a confinement of the plasma is known as hot spot since the electric field in these regions strongly confines the incident field, compared to the smoother surfaces. The field enhancement, in this case, is up to 15 times of the incident field; which is about 2 times that of a Sph NP of similar size.
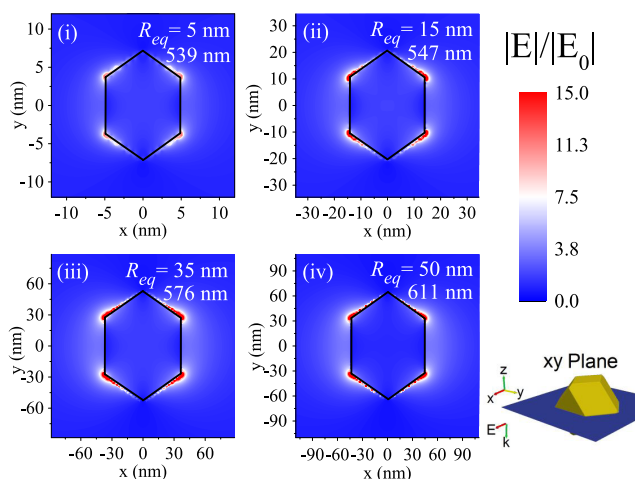
**Figure 4.** Spatial distribution maps of a near electric field for the rhombic dodecahedral gold nanoparticles in the $xy$ plane (see inserted image) for the sizes: (i) $R_{eq}$ = 5 nm, (ii) $R_{eq}$ = 15 nm, (iii) $R_{eq}$ = 35 nm, and (iv) $R_{eq}$ = 50 nm.

Again, the electric field intensity increases as the size increases, however, up to $R_{eq}$ = 35 nm, beyond which it decreases. The observed initial increase of NEF is due to higher absorption of light by bigger NPs, which is maximum for the NP of $R_{eq}$ = 35 nm (Figure S3). The decrease of NEF for the larger NPs is due to their greater light scattering abilities. Although a considerable fraction of the absorbed light by metallic NPs is transformed into an evanescent and nonpropagating near electric field, characteristic for small NPs,[21] a good fraction of the absorbed light in larger NPs is reradiated to the far-field region as scattered (propagating) light.

The near electric field in a Cub NP is mainly localized at the faces parallel to the direction of $E$-polarization, although the hot spots are located at their edges (Figure 5), just as in the case of RhD NP. The intensity of $|E|/|E_0|$ increases up to 8 as the size of Cub NP increases up to $R_{eq}$ = 35 nm, and then decreases following the same trend as for the absorption efficiency factor (Figure S3). However, the $|E|/|E_0|$ is less intense for Cub NP than that of RhD NP, even though the absorption efficiency factor of the former NP is greater than
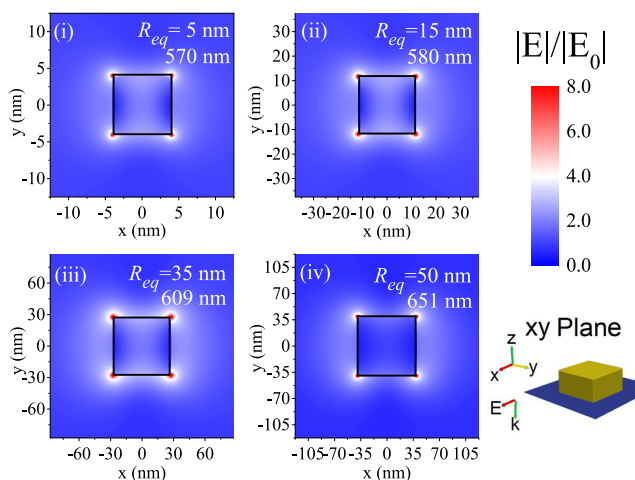
that of the later. This is because the electric field is more localized at the vertices of the RhD NP than in the case of the Cub NP, for these specific orientations of the NPs with respect to the incident electric polarization, which is more convenient for the RhD NP. The oscillating electrons in the case of the Cub NP are not spread at its vertices, but along its edges, resulting in a low electric field localization. Nevertheless, the incident field induces more intense hot spots in the Cub NPs if they are oriented in such a way that the incident electric field is polarized along the Cub NP diagonals, confining a greater number of electrons in a smaller volume at the vertices of the cubes.

In Figure 6, we show the near electric field maps for the aforementioned case, where the position of the cube was
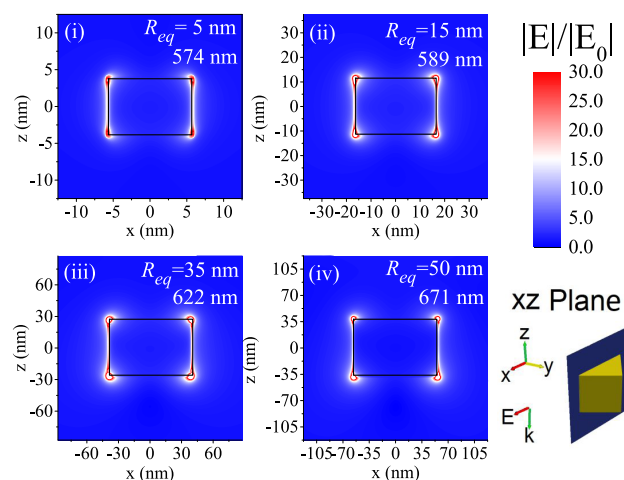


**Figure 6.** Spatial distribution maps of a near electric field in the $xy$ plane (see the inserted image) for the cubic gold nanoparticles rotated by 45° (with respect to Figure 5) of $R_{eq}$ (i) 5 nm, (ii) 15 nm, (iii) 35 nm, and (iv) 50 nm.

rotated 45° with respect to the initial position, and the NEF were calculated at the plane of incidence ($xz$ plane). We can see now that the $|E|/|E_0|$ is around 30 and it is more localized at the vertices, in addition to a lower $|E|/|E_0|$ of approximately 15 along the edges of the cubes. Therefore, the enhancement of the electric field depends greatly on the orientation of the NP for a nonspherical NP. The NEF enhancement of a spherical NP is invariant with respect to polarization and direction of the incident light due to the continuous rotational symmetry of the sphere, the enhancement of nonspherical NPs is orientation dependent because of their discrete rotational symmetry, as can been seen from the electric field maps of the Cub NP with two different orientations presented in Figures 5 and 6. It is well known that the NEFs around elongated−spherical NPs and nanorods are not only dependent of particle orientation but also their aspect ratios, with higher intensities than that for nonelongated nanoparticles.[14] This is very significant in nanostructured materials, where the position and orientation of individual NPs are well controlled to give optical anisotropy to the system for improving their performance in devices. For example, supercrystals and superlattices have been fabricated through self-assembly of polyhedral nanoparticles,[33,34] to amplifying the NEF and use them in SERS, observing higher enhancement factors for RhD NPs in comparison to the enhancement factors obtained using Cub or Oct NPs.[35] Also, the self-assembly of anisotropic nanoparticles (e.g., nanorods)



**Figure 5.** Spatial distribution maps of a near electric field in the $xy$ plane (see the inserted image) for the cubic gold nanoparticles of $R_{eq}$ (i) 5 nm, (ii) 15 nm, (iii) 35 nm, and (iv) 50 nm.

in an ordered superlattice has demonstrated to have different SERS responses, depending on the lattice types (cubic, tetragonal, etc.).[36]

We can also see that the LSPR wavelength has been shifted by 4−20 nm (depending on the size of the NP) as a consequence of reorientation, as the electrons oscillate now over a larger distance (along the cubic diagonal), increasing the retardation effect, i.e., more kinetic energy of the oscillating electrons is lost due to collision, transforming lesser energy to electric field. It has also been observed in elongated nanoparticles, such as nanorods, where two plasmons (longitudinal and transverse modes) could be excited with radiations of different wavelengths, depending on the polarization of the incident light.[37]

Figure 7 shows near electric field enhancement by an Oct NP excited at the dipole mode resonance. As can be seen, the

wavelength is varied from the decapole mode to the dipole mode, because the electrons at the decapole mode are oscillating in more than one direction than in the case of the dipole mode, in which they oscillate in just one direction (along the x-axis) and, therefore, the electric field is more delocalized for the former case.

As it can be noticed from Figures 7, S4, and S6, the near electric field of the Oct NPs is localized mainly at the vertices, irrespective of their size and the nature of the mode (plasmonic) of excitation, as the vertices of the Oct NP are oriented along the polarization direction of the incident electric field. Thanks to this orientation and the sharper borders, the Oct NP has greater NEF enhancement (up to 40 times) than the other three types of NPs mentioned before (Sph, RhD, and Cub NPs).

Finally, the NEF distributions in PBp Au NPs of different sizes are depicted in Figure 8. As can be observed, the



**Figure 7.** Spatial distribution maps of a near electric field in octahedral gold nanoparticles in the xy plane (see inserted image) for equivalent radius ($R_{eq}$) of (i) 5 nm, (ii) 15 nm, (iii) 35 nm, and (iv) 50 nm, under excitation at a corresponding dipole mode resonance.
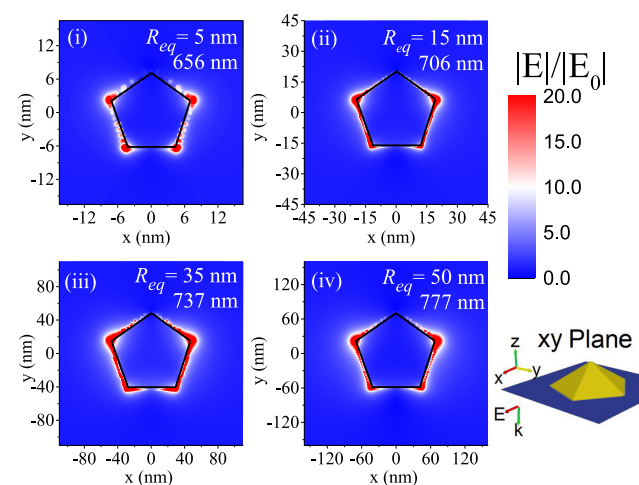


**Figure 8.** Spatial distribution maps of a near electric field for the pentagonal bipyramidal (PBp) gold nanoparticles of different sizes in the xy plane (see inserted image): (1) $R_{eq}$ = 5 nm, (ii) $R_{eq}$ = 15 nm, (iii) $R_{eq}$ = 35 nm, and (iv) $R_{eq}$ = 50 nm, under dipole mode resonance excitation.

NEF in this case is more intense than the NEFs of all of the previous particles (Sph, RhD, and Cub NPs), as the electrons are more localized in the vertex of the octahedron and, therefore, confined in a more reduced space (more intense hot spots).

For the first LSPR band of Oct NP (see Figure S1d) associated to the hexapole mode, the NEF enhancement maps (Figure S4) show a weaker localization of the electric field for each of the four sizes compared with the cases of exciting the NPs at the dipole mode (Figure 7). As can be seen, due to this delocalization of the near electric field, greater amplification (40 times of the incident electric field) is resulted at the dipole mode than for the hexapole mode (30 times).

Although the Oct NPs of $R_{eq}$ in between 5 and 35 nm revealed two resonance modes, the dipole and hexapole, the Oct NPs of $R_{eq}$ = 50 nm manifest one additional plasmon resonance attributed to the decapole mode (see Figure S5a), demonstrating that at this size (and shape), the Oct NP can support all of the three modes.

The NEF maps of the 50 nm Oct NP excited at the three modes (decapole, hexapole, and dipole) are presented in Figure S6. It can be seen that the electric field is more intense and localized at the vertices (which are along the direction of the polarization of the incident electric field) when the

maximum NEF accumulation occurs in the NP of 35 nm equivalent radius, which is about 20 times of the incident electric field intensity. The maximum NEF of this NP is located just at the edges that share the two pentagonal pyramids (see the inserted image), in a very small region. The field in this NP is strongly localized and therefore more intense than in the cases of the Shp, RhD, Cub NPs. Although the field is highly localized in the present case, it is not as localized as in an Oct NP or Cub NP (rotated 45°). A very similar distribution of the electric field is observed for the band associated to its quadrupole mode (Figure S7), but it is less intense than its dipole mode as the electrons, in this case, are more dispersed over the bigger region, as discussed earlier (see the discussion for Oct NP).

From the results obtained for the five analyzed polyhedral NPs, the octahedral NP presents the greater enhancement of the near electric field (40 times), followed by cube (30 times), pentagonal bipyramid (20 times), rhombic dodecahedron (15 times), and the sphere (6 times). As the shape of the metal NP differs from highly symmetric and smooth spherical shape to a shape with less symmetries and rough surface, the electron cloud of the metal NP becomes localized in smaller regions,

resulting in the enhancement of the near electric field. The intensity of the electric field depends also on the orientation of the NP, with respect to the incident field polarization (as it happens in the case of spheroids NP).[38] Moreover, in the nonspherical NPs with sharp borders and/or vertices, the electron cloud remains confined in those narrow regions, forming strong electric hot spots. Therefore, the intensity of the enhanced field depends on the orientation of the NP (which also depends on the shape of the NP) and the nature of exciting polar mode (which is related to the size of the NP). An important consequence of this characteristic is that regular polyhedral NPs could be used as building blocks of photonic superlattices to give them anisotropy-dependent optical properties, as has been reported earlier.[35,36]

The enhanced response of plasmonic NP in SERS-based molecular sensing and other applications has already been demonstrated experimentally.[39] Higher SERS signal for nonspherical NPs, which is proportional to the number of hot spots around the NPs, has also been demonstrated. The signal enhancement also depends on the intensity of these hot spots, i.e., the extent of the electric field localization. As an example, experimentally Zhang et al.[11] have detected 3 times higher SERS signal for the thin film made of octahedral gold nanoparticles in comparison with their thin films made of spherical Au NPs prepared by citrate-mediated reduction.

However, the results obtained by our theoretical calculation indicate that the signal enhancement for octahedral Au NPs should be around 7 times that of spherical Au NPs. The lower signal enhancement detected experimentally might be due to the presence of remained polymer that the authors[11] use to synthetize their Oct NPs, which prevented the efficient interaction between the analytes and the NPs. Moreover, the NPs in their thin films are randomly oriented, reducing the intensity of the hot spots around each of the NPs and, therefore, reducing the total enhancement of a near electric field that they could generate.

## CONCLUSIONS

In summary, we demonstrate that the enhancement of a near electric field around Au nanoparticles strongly depends on their morphology. The more localized are the electrons (or the plasmon), the greater the intensity of the near electric field, and hence the brighter hot spots. Among polyhedral Au NPs studied in this investigation, the highest increase in the electric field occurs for the Oct NPs. However, the region where the electric field is concentrated is very small compared to the intense NEF space of other morphologies. Therefore, for SERS application (for example) of Oct NPs, the analytes must be placed carefully near the faceted areas of the NPs. The more the NPs differ from the spherical shape, the greater their absorption width and dispersion (covering a large range of wavelength). This indicates that polyhedral Au NPs are highly suitable for applications such as in solar cells, where a greater interaction between Au NPs and solar radiation is sought for the wider range of the solar spectrum. In addition, the controlled arrangement of polyhedral NP in a superlattice could give rise to anisotropic optical properties.

## ASSOCIATED CONTENT

**⑤ Supporting Information**

The Supporting Information is available free of charge on the ACS Publications website at DOI: 10.1021/acs.jpcc.9b01105.

Parameters used to calculate the optical properties of Au NPs (Table S1); extinction efficiency factors of Au NPs of different shapes and sizes (Figure S1); electric charge density on the $xy$ plane of the Au NPs with $R_{eq}$ = 5 nm (Figure S2); maximum of the absorption efficiency factors of the Au NPs with the considered shapes and sizes (Figure S3); NEF maps of Oct NPs at the hexapole resonance for different sizes and the NEF maps of Oct NP for $R_{eq}$ = 50 nm at the dipole, hexapole, and decapole modes (Figures S4 and S6); electric charge density on the $xy$ plane of the Oct NP with $R_{eq}$ = 50 nm (Figure S5); NEF maps of PBp NPs at the quadrupole resonance for different sizes (Figure S7) (PDF)

## AUTHOR INFORMATION

**Corresponding Author**

*E-mail: upal@ifuap.buap.mx. Fax: +52-222-2295611.

**ORCID** ⊙

Umapada Pal: 0000-0002-5665-106X

**Notes**

The authors declare no competing financial interest.

## REFERENCES

(1) Chatterjee, D. K.; Diagaradjane, P.; Krishnan, S. Nanoparticle-Mediated Hyperthermia in Cancer Therapy. *Ther. Delivery* **2011**, *2*, 1001−1014.

(2) Lane, L. A.; Qian, X.; Nie, S. SERS Nanoparticles in Medicine: From Label-Free Detection to Spectroscopic Tagging. *Chem. Rev.* **2015**, *115*, 10489−10529.

(3) Enrichi, F.; Quandt, A.; Righini, G. C. Plasmonic Enhanced Solar Cells: Summary of Possible Strategies and Recent Results. *Renewable Sustainable Energy Rev.* **2018**, *82*, 2433−2439.

(4) Montaño-Priede, J. L.; Peña-Rodríguez, O.; Pal, U. Near-Electric-Field Tuned Plasmonic Au@SiO₂ and Ag@SiO₂ Nanoparticles for Efficient Utilization in Luminescence Enhancement and Surface-Enhanced Spectroscopy. *J. Phys. Chem. C* **2017**, *121*, 23062−23071.

(5) Montaño-Priede, L.; Peña-Rodríguez, O.; Rivera, A.; Guerrero-Martínez, A.; Pal, U. Optimizing the Electric Field around Solid and Core−Shell Alloy Nanostructures for Near-Field Applications. *Nanoscale* **2016**, *8*, 14836−14845.

(6) Noguez, C. Surface Plasmons on Metal Nanoparticles: The Influence of Shape and Physical Environment. *J. Phys. Chem. C* **2007**, *111*, 3806−3819.

(7) Grzelczak, M.; Pérez-Juste, J.; Mulvaney, P.; Liz-Marzán, L. M. Shape Control in Gold Nanoparticle Synthesis. *Chem. Soc. Rev.* **2008**, *37*, 1783−1791.

(8) Zhao, T.-T.; Wang, H.; Han, X.; Jiang, K.; Lin, H.; Xie, Z.; Cai, W.-B. A Comparative Investigation of Electrocatalysis at Pt Monolayers on Shape-Controlled Au Nanocrystals: Facet Effect versus Strain Effect. *J. Mater. Chem. A* **2016**, *4*, 15845−15850.

(9) Dreaden, E. C.; Alkilany, A. M.; Huang, X.; Murphy, C. J.; El-Sayed, M. A. The Golden Age: Gold Nanoparticles for Biomedicine. *Chem. Soc. Rev.* **2012**, *41*, 2740−2779.

(10) Liu, Y.; Zhou, J.; Yuan, X.; Jiang, T.; Petti, L.; Zhou, L.; Mormile, P. Hydrothermal Synthesis of Gold Polyhedral Nanocrystals

by Varying Surfactant Concentration and Lheir LSPR and SERS Properties. *RSC Adv.* **2015**, *5*, 68668−68675.

(11) Zhang, J.; Gao, Y.; Alvarez-Puebla, R. A.; Buriak, J. M.; Fenniri, H. Synthesis and SERS Properties of Nanocrystalline Gold Octahedra Generated from Thermal Decomposition of HAuCl₄ in Block Copolymers. *Adv. Mater.* **2006**, *18*, 3233−3237.

(12) Chen, Y.; Gu, X.; Nie, C.-G.; Jiang, Z.-Y.; Xie, Z.-X.; Lin, C.-J. Shape Controlled Growth of Gold Nanoparticles by a Solution Synthesis. *Chem. Commun.* **2005**, 4181−4183.

(13) Kuo, B.-H.; Hsia, C.-F.; Chen, T.-N.; Huang, M. H. Systematic Shape Evolution of Gold Nanocrystals Achieved through Adjustment in the Amount of HAuCl₄ Solution Used. *J. Phys. Chem. C* **2018**, *122*, 25118−25126.

(14) Noguez, C.; Villagómez, C. J.; González, A. L. Plasmonics of multifaceted metallic nanoparticles, field enhancement, and TERS. *Phys. Satus Solidi B* **2015**, *252*, 56−71.

(15) Cobley, C. M.; Skrabalak, S. E.; Campbell, D. J.; Xia, Y. Shape-Controlled Synthesis of Silver Nanoparticles for Plasmonic and Sensing Applications. *Plasmonics* **2009**, *4*, 171−179.

(16) Noguez, C.; Gonzalez, A. L. Localized Surface Plasmons of Multifaceted Metal Nanoparticles. In *Complex-Shaped Metal Nanoparticles*; Sau, T. K., Rogach, A. L., Eds.; Wiley, 2012; Vol. *2012*, pp 361−393.

(17) Pastoriza-Santos, I.; Liz-Marzan, L. M. N, N-Dimethylformamide as a Reaction Medium for Metal Nanoparticle Synthesis. *Adv. Funct. Mater* **2009**, *19*, 679−688.

(18) Sun, Y.; Xia, Y. Shape-Controlled Synthesis of Gold and Silver Nanoparticles. *Science* **2002**, *298*, 2176−2179.

(19) Lu, Y.; Zhang, H.; Wu, F.; Liu, H.; Fang, J. Size-Tunable Uniform Gold Octahedra: Fast Synthesis, Characterization, and Plasmonic Properties. *RSC Adv.* **2017**, *7*, 18601−18608.

(20) Zaleska-Medynska, A.; Marchelek, M.; Diak, M.; Grabowska, E. Noble Metal-Based Bimetallic Nanoparticles: The Effect of the Structure on the Optical, Catalytic and Photocatalytic Properties. *Adv. Colloid Interface Sci.* **2016**, *229*, 80−107.

(21) Choi, K. W.; Kim, D. Y.; Zhong, X.-L.; Li, Z.-Y.; Im, S. H.; Park, O. O. Robust Synthesis of Gold Rhombic Dodecahedra with Well-Controlled Sizes and Their Optical Properties. *CrystEngComm* **2013**, *15*, 252−258.

(22) Zhang, Q.; Large, N.; Nordlander, P.; Wang, H. Porous Au Nanoparticles with Tunable Plasmon Resonances and Intense Field Enhancements for Single-Particle SERS. *J. Phys. Chem. Lett.* **2014**, *5*, 370−37.

(23) Kwon, K.; Lee, K. Y.; Kim, M.; Lee, Y. W.; Heo, J.; Ahn, S. J.; Han, S. W. High-Yield Synthesis of Monodisperse Polyhedral Gold Nanoparticles with Controllable Size and Their Surface-Enhanced Raman Scattering Activity. *Chem. Phys. Lett.* **2006**, *432*, 209−212.

(24) Oskooi, A. F.; Roundy, D.; Ibanescu, M.; Bermel, P.; Joannopoulos, J.; Johnson, S. G. MEEP: A Flexible Free-Software Package for Electromagnetic Simulations by the FDTD Method. *Comput. Phys. Commun.* **2010**, *181*, 687−702.

(25) Jeong, G. H.; Kim, M.; Lee, Y. W.; Choi, W.; Oh, W. T.; Park, Q.-H.; Han, S. W. Polyhedral Au Nanocrystals Exclusively Bound by {110} Facets: The Rhombic Dodecahedron. *J. Am. Chem. Soc.* **2009**, *131*, 1672−1673.

(26) Johnson, P. B.; Christy, R. W. Optical Constants of the Noble Metals. *Phys. Rev. B* **1972**, *6*, 4370−4379.

(27) Niu, W.; Zheng, S.; Wang, D.; Liu, X.; Li, H.; Han, S.; Chen, J.; Tang, Z.; Xu, G. Selective Synthesis of Single-Crystalline Rhombic Dodecahedral, Octahedral, and Cubic Gold Nanocrystals. *J. Am. Chem. Soc.* **2009**, *131*, 697−703.

(28) Personick, M. L.; Langille, M. R.; Zhang, J.; Harris, N.; Schatz, G. C.; Mirkin, C. A. Synthesis and Isolation of {110}-Faceted Gold Bipyramids and Rhombic Dodecahedra. *J. Am. Chem. Soc.* **2011**, *133*, 6170−6173.

(29) Li, C.; Shuford, K. L.; Chen, M.; Lee, E. J.; Cho, S. O. A Facile Polyol Route to Uniform Gold Octahedra with Tailorable Size and Their Optical Properties. *ACS Nano* **2008**, *2*, 1760−1769.

(30) Zhang, X.; Tsuji, M.; Lim, S.; Miyamae, N.; Nishio, M.; Hikino, S.; Umezu, M. Synthesis and Growth Mechanism of Pentagonal Bipyramid-Shaped Gold-Rich Au/Ag Alloy Nanoparticles. *Langmuir* **2007**, *23*, 6372−6376.

(31) González, A. L.; Noguez, C. Optical Properties of Silver Nanoparticles. *Phys. Status Solidi C* **2007**, *4*, 4118−4126.

(32) Kelly, K. L.; Coronado, E.; Zhao, L. L.; Schatz, G. C. The Optical Properties of Metal Nanoparticles: The Influence of Size, Shape, and Dielectric Environment. *J. Phys. Chem. B* **2003**, *107*, 668−677.

(33) Huang, M. H.; Thoka, S. Formation of Supercrystals Through Self-Assembly of Polyhedral Nanocrystals. *Nano Today* **2015**, *10*, 81−92.

(34) Ross, M. B.; Ku, J. C.; Vaccarezza, V. M.; Schatz, G. C.; Mirkin, C. A. Nanoscale Form Dictates Mesoscale Function in Plasmonic DNA−Nanoparticle Superlattices. *Nat. Nanotechnol.* **2015**, *10*, 453−458.

(35) Wu, H. -L; Tsai, H.-R.; Hung, Y.-T.; Lao, K.-U.; Liao, C.-W.; Chung, P.-J.; Huang, J.-S.; Chen, I-C.; Huang, M. H. A Comparative Study of Gold Nanocubes, Octahedra, and Rhombic Dodecahedra as Highly Sensitive SERS Substrates. *Inorg. Chem.* **2011**, *50*, 8106−8111.

(36) Liang, Y.; Xie, Y.; Chen, D.; Guo, C.; Hou, S.; Wen, T.; Yang, F.; Deng, K.; Wu, X.; Smalyukh, I. I.; Liu, Q. Symmetry Control of Nanorod Superlattice Driven by a Governing Force. *Nat. Commun.* **2017**, *8*, No. 1410.

(37) Tong, W.; Walsh, M. J.; Mulvaney, P.; Etheridge, J.; Funston, A. M. Control of Symmetry Breaking Size and Aspect Ratio in Gold Nanorods: Underlying Role of Silver Nitrate. *J. Phys. Chem. C* **2017**, *121*, 3549−3559.

(38) Sendur, K.; Sahinöz, A. Interaction of Radially Polarized Focused Light with a Prolate Spheroidal Nanoparticle. *Opt. Express* **2009**, *17*, 10910−10925.

(39) Tian, F.; Bonnier, F.; Casey, A.; Shanahan, A. E.; Byrne, H. J. Surface Enhanced Raman Scattering with Gold Nanoparticles: Effect of Particle Shape. *Anal. Methods* **2014**, *6*, 9116−9123.